AMERICAN SOCIETY FOR MICROBIOLOGY | Journal of Virology®

VACCINES AND ANTIVIRAL AGENTS

Insight into Vaccine Development for Alphacoronaviruses Based on Structural and Immunological Analyses of Spike Proteins

Yuejun Shi,[a,b] Jiale Shi,[a,b] Limeng Sun,[a,b] Yubei Tan,[a,b] Gang Wang,[a,b] Fenglin Guo,[a,b] Guangli Hu,[a,b] Yanan Fu,[a,b] Zhen F. Fu,[a,b,c] Shaobo Xiao,[a,b] Guiqing Peng[a,b]

[a]State Key Laboratory of Agricultural Microbiology, College of Veterinary Medicine, Huazhong Agricultural University, Wuhan, China
[b]Key Laboratory of Preventive Veterinary Medicine in Hubei Province, The Cooperative Innovation Center for Sustainable Pig Production, Wuhan, China
[c]Department of Pathology, College of Veterinary Medicine, University of Georgia, Athens, Georgia, USA

Yuejun Shi, Jiale Shi, and Limeng Sun contributed equally to this work. Author order was determined both alphabetically and in order of increasing seniority.

ABSTRACT Coronaviruses that infect humans belong to the *Alphacoronavirus* (including HCoV-229E) and *Betacoronavirus* (including SARS-CoV and SARS-CoV-2) genera. In particular, SARS-CoV-2 is currently a major threat to public health worldwide. The spike (S) homotrimers bind to their receptors via the receptor-binding domain (RBD), which is a major target to block viral entry. In this study, we selected *Alphacoronavirus* (HCoV-229E) and *Betacoronavirus* (SARS-CoV and SARS-CoV-2) as models. Their RBDs exist two different conformational states ("lying" or "standing") in the prefusion S-trimer structure. Then, the differences in the immune responses to RBDs from these coronaviruses were analyzed structurally and immunologically. Our results showed that more RBD-specific antibodies (antibody titers: 1.28×10^5 and 2.75×10^5, respectively) were induced by the S-trimer with the RBD in the standing state (SARS-CoV and SARS-CoV-2) than the S-trimer with the RBD in the lying state (HCoV-229E; antibody titers: <500), and more S-trimer-specific antibodies were induced by the RBD in the SARS-CoV and SARS-CoV-2 (antibody titers: 6.72×10^5 and 5×10^5, respectively) than HCoV-229E (antibody titers: 1.125×10^3). Besides, we found that the ability of the HCoV-229E RBD to induce neutralizing antibodies was lower than S-trimer, and the intact and stable S1 subunit was essential for producing efficient neutralizing antibodies against HCoV-229E. Importantly, our results reveal different vaccine strategies for coronaviruses, and S-trimer is better than RBD as a target for vaccine development in *Alphacoronavirus*. Our findings will provide important implications for future development of coronavirus vaccines.

IMPORTANCE Outbreaks of coronaviruses, especially SARS-CoV-2, pose a serious threat to global public health. Development of vaccines to prevent the coronaviruses that can infect humans has always been a top priority. Coronavirus spike (S) protein is considered a major target for vaccine development. Currently, structural studies have shown that *Alphacoronavirus* (HCoV-229E) and *Betacoronavirus* (SARS-CoV and SARS-CoV-2) RBDs are in "lying" and "standing" states in the prefusion S-trimer structure. Here, we evaluated the ability of S-trimer and RBD to induce neutralizing antibodies among these coronaviruses. Our results showed that the S-trimer and RBD are both candidates for subunit vaccines in *Betacoronavirus* (SARS-CoV and SARS-CoV-2) with an RBD standing state. However, for *Alphacoronavirus* (HCoV-229E) with an RBD lying state, the S-trimer may be more suitable for subunit vaccines than the RBD. Our results will provide novel ideas for the development of vaccines targeting S protein in the future.

KEYWORDS coronavirus, spike protein, receptor-binding domain, structural analysis, neutralizing antibody

Citation Shi Y, Shi J, Sun L, Tan Y, Wang G, Guo F, Hu G, Fu Y, Fu ZF, Xiao S, Peng G. 2021. Insight into vaccine development for alphacoronaviruses based on structural and immunological analyses of spike proteins. J Virol 95:e02284-20. https://doi.org/10.1128/JVI.02284-20.

Editor Tom Gallagher, Loyola University Chicago

Address correspondence to Guiqing Peng, penggq@mail.hzau.edu.cn.

Received 30 November 2020
Accepted 21 December 2020
Accepted manuscript posted online 7 January 2021
Published 10 March 2021

Coronaviruses (CoVs) are enveloped, positive-sense, single-stranded RNA viruses with the largest genomes (26 to 32 kb) among known RNA viruses and are phylogenetically divided into four genera (*Alpha-*, *Beta-*, *Gamma-*, and *Deltacoronavirus*) (1, 2). To date, seven human-infecting coronaviruses (hCoVs) (3, 4) cause various degrees of symptoms: HCoV-229E, HCoV-NL63, HCoV-HKU1, HCoV-OC43, severe acute respiratory syndrome coronavirus (SARS-CoV), Middle East respiratory syndrome coronavirus (MERS-CoV), and SARS-CoV-2, which caused the current epidemic of COVID-19. Among them, alpha-CoVs (HCoV-229E and HCoV-NL63) and beta-CoVs (HCoV-OC43 and HCoV-HKU1) are well adapted to humans and widely circulate in the human population, with most infections causing mild disease in immunocompetent adults (3, 5, 6). In addition, SARS-CoV, SARS-CoV-2, and MERS-CoV belong to *Beta-CoV* and are highly pathogenic (7–9). SARS-CoV emerged in 2002 and spread worldwide, resulting in 8,273 infections and nearly 775 deaths, with an approximately 9% case fatality rate (CFR) (9). MERS-CoV emerged in 2012 and caused numerous outbreaks in humans, with an approximately 36% CFR (10). SARS-CoV-2 is a newly emerged coronavirus strain (4), which has resulted in more than 70 million infections worldwide and more than 1 million deaths (https://www.who.int/emergencies/diseases/novel-coronavirus-2019).

As the primary glycoprotein on the surface of the viral envelope, the spike (S) glycoprotein contains two subunits responsible for receptor binding (S1 subunit) and membrane fusion (S2 subunit) (11). In particular, the S1 subunit of the prefusion S protein is structurally organized into four distinct domains: the N-terminal domain (NTD), the C-terminal domain (CTD), subdomain 1 (SD1), and subdomain 2 (SD2) (12–24). The receptor-binding domain (RBD) in the S protein mediates the binding of the virus to host cells, which is a critical step for the virus to enter target cells (11, 25). The CTDs of alpha-CoVs HCoV-NL63 and HCoV-229E are used as RBDs, which bind to angiotensin-converting enzyme 2 (ACE2) and aminopeptidase (APN), respectively (26, 27). The CTDs of beta-CoVs (SARS-CoV, SARS-CoV-2, and MERS-CoV) are similar in their core structures but are markedly different in their receptor-binding motifs (RBMs), leading to different receptor specificities; SARS-CoV and SARS-CoV-2 recognize ACE2 (28, 29), whereas MERS-CoV recognizes dipeptidyl peptidase-4 (DPP4) (30).

Currently, the S-trimer structures in the prefusion state have been reported for members of alpha-CoVs (HCoV-NL63, HCoV-229E, porcine epidemic diarrhea virus [PEDV], and feline infectious peritonitis [FIPV]) (12, 14, 16, 22), Beta-CoVs (mouse hepatitis virus [MHV], HCoV-HKU1, HCoV-OC43, SARS-CoV, SARS-CoV-2, and MERS-CoV) (13, 15, 20, 21, 23, 24), gamma-CoV (avian coronavirus [infectious bronchitis coronavirus {IBV}]) (19), and delta-CoV (porcine deltacoronavirus [PDCoV]) (17, 18). The S1 subunits of *Beta-* and *Gamma-CoV* strains utilize the cross-subunit packing mode, reducing the conformational conflict of the RBD in a "standing" state (13, 19–21). In contrast, *Alpha-* and *Delta-CoV* strains both utilize an intrasubunit packing mode, and the S1-CTD is limited by the conformational conflict with surrounding domains (12, 14, 16–19, 22). Hence, the S1-RBD in the S-trimer was captured in two different states among different coronaviruses. In the beta-CoVs (SARS-CoV, SARS-CoV-2, and MERS-CoV), the S1-CTD adopts a standing state, which is believed to be a prerequisite for receptor binding and RBM-specific antibody binding (13, 20, 21). Nevertheless, the S1-CTDs of alpha-CoVs all adopt the "lying" state, which is considered more conducive to evading antibody recognition (12, 14, 16, 22).

Currently, a number of subunit vaccines targeting S protein or RBD have been developed against SARS-CoV, SARS-CoV-2, and MERS-CoV (31–36). Compared with beta-CoVs, relatively few studies have investigated two alpha-hCoVs: HCoV-229E and HCoV-NL63. Besides, their S1 subunit structure and receptor recognition pattern, especially the structure of the RBD and its state in the S-trimer, differ substantially from those of beta-CoVs, suggesting different S protein immune responses between alpha- and beta-CoVs. Importantly, considering the low homology between different coronavirus genera, related research on alpha-CoVs can not only help to elucidate the differences between S proteins that adopt different RBD conformational states but can also

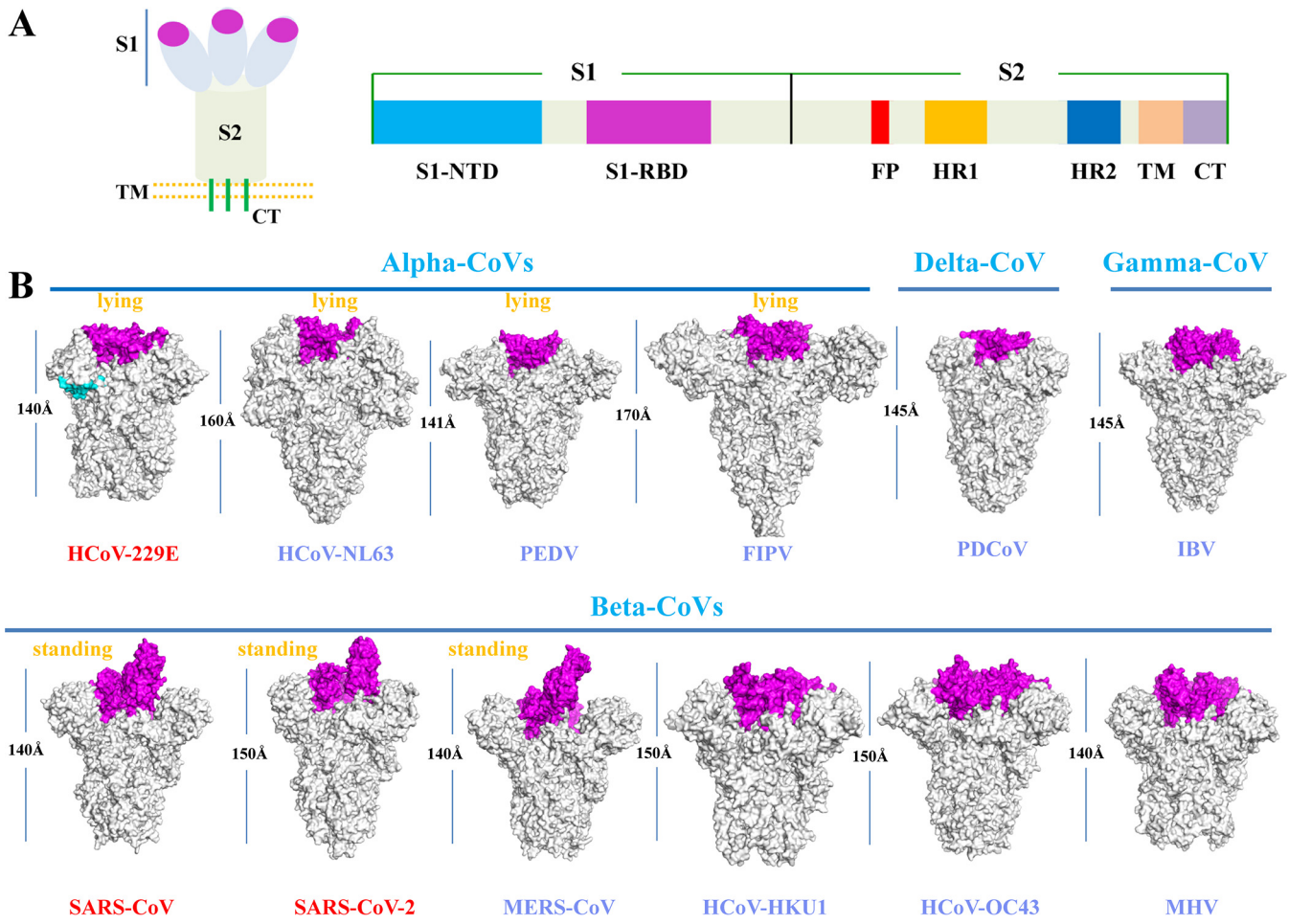

FIG 1 Structural analysis of S1-RBDs from coronavirus S-trimers. (A) Schematic diagram of coronavirus spike protein organization. S1, receptor-binding subunit; S2, membrane fusion subunit; NTD, N-terminal domain; RBD, receptor-binding domain; FP, fusion peptide; HR1, heptad repeat 1; HR2, heptad repeat 2; TM, transmembrane domain; CT, cytoplasmic tail. (B) Overall structure comparison of coronavirus S-trimers. The S-trimer structures of HCoV-229E (PDB ID: 6U7H), HCoV-NL63 (PDB ID: 5SZS), PEDV (PDB ID: 6U7K), FIPV (PDB ID: 6JX7), PDCoV (PDB ID: 6BFU), IBV (PDB ID: 6CV0), SARS-CoV (PDB ID: 5X5B), SARS-CoV-2 (PDB ID: 6VSB), MERS-CoV (PDB ID: 5X5F), HCoV-HKU1 (PDB ID: 5I08), HCoV-OC43 (PDB ID: 6OHW), and mouse hepatitis virus (MHV) (PDB ID: 3JCL) are shown. The S1-RBDs are colored in magenta. The lengths of the coronavirus S-trimers are shown as previously reported.

facilitate the development of coronavirus vaccines. In this study, we selected SARS-CoV, SARS-CoV-2, and HCoV-229E as models, which exist in two RBD conformational states, and evaluated the ability of S-trimer and RBD to induce neutralizing antibodies. Moreover, we provide possible vaccine strategies for alpha- and beta-CoVs, which may facilitate the design and development of coronavirus vaccines in the future.

RESULTS AND DISCUSSION

Structural and immunological analyses of alpha- and beta-coronavirus spike proteins. To date, multiple S-trimer structures of coronaviruses have been resolved (12–24). Through structural comparison, we found that although the amino acid sequences are quite different, the compositions and structures of different functional domains of coronaviruses are consistent (Fig. 1A). All the alpha-CoVs bind to protein receptors with CTDs (as receptor-binding domains [RBDs]), and the RBDs are in a lying state (12, 14, 16, 22, 26, 27) (Fig. 1B). However, beta-CoVs (SARS-CoV, SARS-CoV-2, and MERS-CoV) bind receptors with CTDs (as RBDs), and the RBDs are in a standing state (13, 20, 21) (Fig. 1B). The RBD directly binds to receptors, which is an important target for the induction of neutralizing antibody (NAb).

Then, we performed B-cell epitope predictions for the S-trimers and RBDs of alpha-CoV (HCoV-229E) and beta-CoVs (SARS-CoV and SARS-CoV-2). The predicted positive

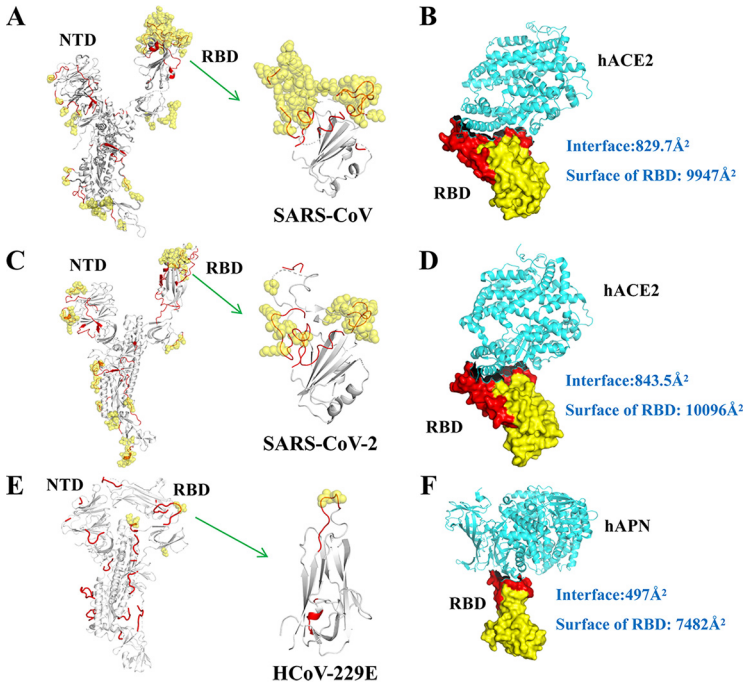

FIG 2 Structure-based B-cell epitope predictions of *Beta-CoV* (SARS-CoV and SARS-CoV-2) and *Alpha-CoV* (HCoV-229E). (A, C, and E) The predicted B-cell epitopes of SARS-CoV, SARS-CoV-2, and HCoV-229E are shown. The linear (red cartoon) and conformational (yellow sphere) B-cell epitopes were predicted using Bepipred 2.0 or DiscoTope 2.0 and labeled into the corresponding structure via PyMOL. (B, D, and F) The complex structures of the RBDs of SARS-CoV (PDB ID: 2AJF), SARS-CoV-2 (PDB ID: 6M0J), and HCoV-229E (PDB ID: 6ATK) with the receptors (hACE2 and hAPN) are shown. The interface area and the surface area were calculated via PDBePISA. The RBM region of the RBD and the receptors (hACE2 and hAPN) are shown in red and cyan, respectively.

residues (the corresponding spatial epitope and linear epitope) are displayed on the structural surface (Fig. 2A, C, and E), and the distribution of positive residues on the RBD is summarized in Table 1. A total of 51 and 26 amino acid residues located on the RBD were predicted to be conformational epitopes for SARS-CoV and SARS-CoV-2, respectively. Of these, 47 and 25 residues were located in the RBM subdomains of SARS-CoV and SARS-CoV-2, respectively. The linear B-cell epitope prediction results were similar in SARS-CoV and SARS-CoV-2. However, in HCoV-229E, only 3 residues located in the RBM subdomain were predicted to be conformational epitopes, and 9 residues were predicted to be linear epitopes. The same results also appeared in the HCoV-229E S-trimer; fewer positive residues were located in the RBD than in the SARS-CoV or SARS-CoV-2 RBM subdomain (Fig. 2A, C and E). Meanwhile, we analyzed the

TABLE 1 Distribution of residues predicted positive for B-cell epitopes

	No. of residues				
	RBD		RBM		
Virus	Conformational	Linear	Conformational	Linear	RBM/RBD ratio (%)
SARS-CoV	51	56	47	33	92.2/58.9
SARS-CoV-2	26	59	25	35	96.2/59.3
HCoV-229E	3	14	3	9	100/64.3
HCoV-NL63	4	33	4	19	100/57.6
PRCoV	4	41	4	27	100/65.9
TGEV	7	34	4	24	57.1/70.6
PEDV	0	21	0	8	0/38.1
FIPV	0	17	0	11	0/64.7

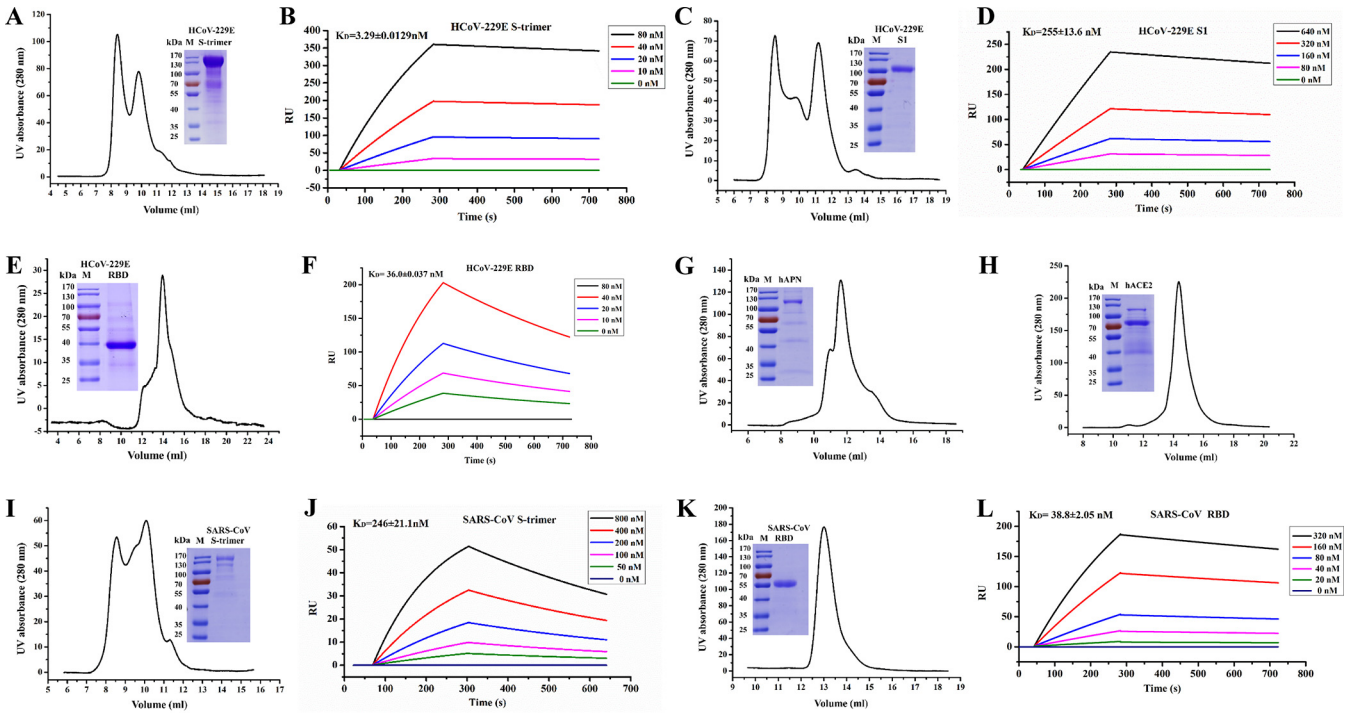

FIG 3 Surface plasmon resonance binding data for the interaction between the coronavirus spike proteins and the receptors. (A, C, E, G, H, I, and K) Oligomerization state analysis of spike proteins (HCoV-229E: S-trimer, S1, and RBD; SARS-CoV: S-trimer and RBD) and the receptors (hAPN and hACE2). Protein samples were eluted using a Superdex 200 10/300 GL column. The results of SDS-PAGE analysis are also shown. (B, D, F, J, and L) Interactions of spike proteins and soluble hAPN and hACE2. Purified recombinant hAPN or hACE2 was covalently immobilized on the OpenSPR COOH sensor chip via its amine groups, and purified recombinant spike proteins were made to flow over the hAPN or hACE2. Response unit (RU) values were measured at 298 K. Binding kinetics was evaluated using a 1:1 Langmuir binding model; binding constants are indicated. All injections were carried out in duplicate and gave essentially identical results. Only one of the duplicates is shown.

binding area of the RBD and receptors from SARS-CoV, SARS-CoV-2, and HCoV-229E (Fig. 2B, D, and F). Among them, the interaction areas of SARS-CoV and SARS-CoV-2 were similar (approximately 829.7 Å^2 and 843.5 Å^2, respectively) and were larger than that of HCoV-229E (approximately 497 Å^2). Furthermore, surface area analysis also yielded consistent results (Fig. 2B, D, and F). Compared with HCoV-229E, the larger surface areas and binding areas of the SARS-CoV and SARS-CoV-2 RBDs to the receptor may induce more NAbs. The cryo-electron microscopy (cryo-EM) structures of S-trimers in the prefusion conformation have shown that the SARS-CoV and SARS-CoV-2 RBDs are in a standing state (13, 20, 21); however, HCoV-229E RBDs are in a lying state (16) (Fig. 1B). Hence, compared with HCoV-229E, this may make it difficult for SARS-CoV and SARS-CoV-2 to evade neutralizing antibodies that target RBD recognition.

Distinct immunogenicity of the RBDs in *Alpha-CoV* (HCoV-229E) and *Beta-CoV* (SARS-CoV and SARS-CoV-2). To evaluate the immunogenicity of the S-trimers and RBDs between *Alpha-CoV* (HCoV-229E) and *Beta-CoV* (SARS-CoV and SARS-CoV-2), the recombinant S proteins were expressed and purified (Fig. 3A, E, I, and K). Because the prefusion-stabilized S proteins could influence RBD standing or lying conformational states, two proline substitutions in the loop between the heptad repeat (HR1) and the central helix (CH) have not been introduced (31, 37). For *in vitro* binding measurements (Fig. 3B, F, J, and L; Table 2), the equilibrium dissociation constants (K_Ds) of HCoV-229E spike proteins (S-trimer and RBD) and hAPN are 3.29 $\pm$ 0.0129 nM and 36.0 $\pm$ 0.037 nM, respectively. Besides, the K_D values of SARS-CoV spike proteins (S-trimer and RBD) and hACE2 are 246 $\pm$ 21.1 nM and 38.8 $\pm$ 2.05 nM, respectively. Compared with previous research (26), our results showed that all the spike proteins function well *in vitro*. Then, the S-trimer (10 μg) and RBD (10 μg) were used as antigens to immunize mice. The antibody response was measured via enzyme-linked immunosorbent assay (ELISA) using collected sera. The data showed that the S-trimer and RBD of SARS-CoV and

TABLE 2 Surface plasmon resonance binding data for the interaction between the coronavirus (HCoV-229E and SARS-CoV) spike proteins and the receptors (hAPN and hACE2)[a]

Virus	Spike protein	K_{on} ($\times 10^4$ M^{-1} s^{-1})	K_{off} ($\times 10^{-4}$ s^{-1})	K_D (nM)
HCoV-229E	S-trimer	3.67 ± 0.0005	1.21 ± 0.0046	3.29 ± 0.0129
	S trimer/ΔNTD	1.94 ± 0.0006	0.41 ± 0.0289	2.12 ± 0.15
	S1	0.0886 ± 0.0006	2.26 ± 0.104	255 ± 13.6
	S1-RBD	3.2 ± 0.00174	11.5 ± 0.0056	36.0 ± 0.037
SARS-CoV	S-trimer	0.622 ± 0.0499	15.3 ± 0.0755	246 ± 21.1
	S1-RBD	0.812 ± 0.0004	3.15 ± 0.165	38.8 ± 2.05

[a]Values after ± correspond to the residual standard deviation. Each experiment was repeated independently twice with similar results.

SARS-CoV-2 could induce high levels of protein-specific antibodies (antibody titers: 1.36×10^5 and 3.84×10^5, and 1.625×10^6 and 5×10^5, respectively) (Fig. 4A to D). Moreover, the S-trimers of both SARS-CoV and SARS-CoV-2 could induce high-titer RBD antibodies (antibody titers: 1.28×10^5 and 2.75×10^5, respectively) (Fig. 4B and D), and the RBD could induce high-titer S-trimer antibodies (antibody titers: 6.72×10^5 and 5×10^5, respectively) (Fig. 4A and C). Similar to SARS-CoV and SARS-CoV-2, the S-trimer and RBD of HCoV-229E both had good immunogenicity (antibody titers: 8.8×10^4 and 7.68×10^5, respectively) (Fig. 4E and F). However, the HCoV-229E S-trimer induced fewer RBD-specific antibodies than those of SARS-CoV and SARS-CoV-2 (antibody titer: $<$500) (Fig. 4F), and the HCoV-229E RBD induced low-titer S-trimer antibodies (antibody titer: 1.125×10^3) (Fig. 4E and H). To confirm this finding, a higher immunization dose of the HCoV-229E RBD (50 μg) was used in the same manner. Nevertheless, no significant increase in the RBD-specific antibody titer (antibody titers: 1.792×10^6 and 3.072×10^6) (Fig. 3G) or antibody titer for the HCoV-229E S-trimer (antibody titers: 2.5×10^2 and 2.5×10^2) (Fig. 3H) was noted. Overall, our immune epitope analysis and biochemical tests consistently showed that the S-trimer with a standing RBD state is more conducive to inducing RBD-specific antibodies in SARS-CoV and SARS-CoV-2. However, the S-trimer with a lying RBD state induces fewer RBD-specific antibodies in HCoV-229E.

HCoV-229E RBD induced fewer specific neutralizing antibodies than those of SARS-CoV and SARS-CoV-2. Next, we tested the neutralizing ability of the sera using a vesicular stomatitis virus (VSV)-based pseudovirus (100 50% tissue culture infective doses [$TCID_{50}$]/well). Both the S-trimer and RBD sera from SARS-CoV- and SARS-CoV-2-immunized mice had a good neutralizing ability (Fig. 4I and J). For HCoV-229E, the S-trimer sera had a neutralizing ability comparable to that of SARS-CoV or SARS-CoV-2, but the RBD sera had no detectable neutralizing ability (Fig. 4K). Based on the results, we speculate that the antibodies induced by HCoV-229E RBD contain only a small part of neutralizing antibodies, which may be the reason for the weak ability of RBD sera to neutralize viruses. In HCoV-229E, the distribution of the potential B-cell epitopes in the RBD was lower than that of SARS-CoV or SARS-CoV-2 (Fig. 2A, C, and E; Table 1), which may have caused fewer NAbs to be induced by the RBD. Therefore, we believe that this finding illustrates the inherent difference between the RBDs of *alpha-* and *betaCoV*. Besides, our results indicate that HCoV-229E S-trimer induces the production of very few antibodies targeting the RBD (antibody titer: $<$500) (Fig. 4F), but the S-trimer still produces strong neutralizing antibody levels; the mechanism needs further clarification.

The intact and stable S1 subunit in HCoV-229E S-trimer is a prerequisite for the production of effective NAbs. Our experimental results showed that the HCoV-229E S-trimer can induce high NAb levels, while the RBD alone is less immunogenic. Then, we explored which functional domains of the S-trimer are involved in the generation of NAbs. To clarify this issue, we immunized mice with the HCoV-229E S-trimer (10 μg), S1 (10 μg [Fig. 3C and D]), NTD (10 μg [Fig. 5A]), RBD (10 μg), and NTD+RBD (5 μg + 5 μg). Besides, the HCoV-229E strain VR740 was used for the neutralizing assay. Our results indicated that the S-trimer sera had the best neutralizing ability, followed by

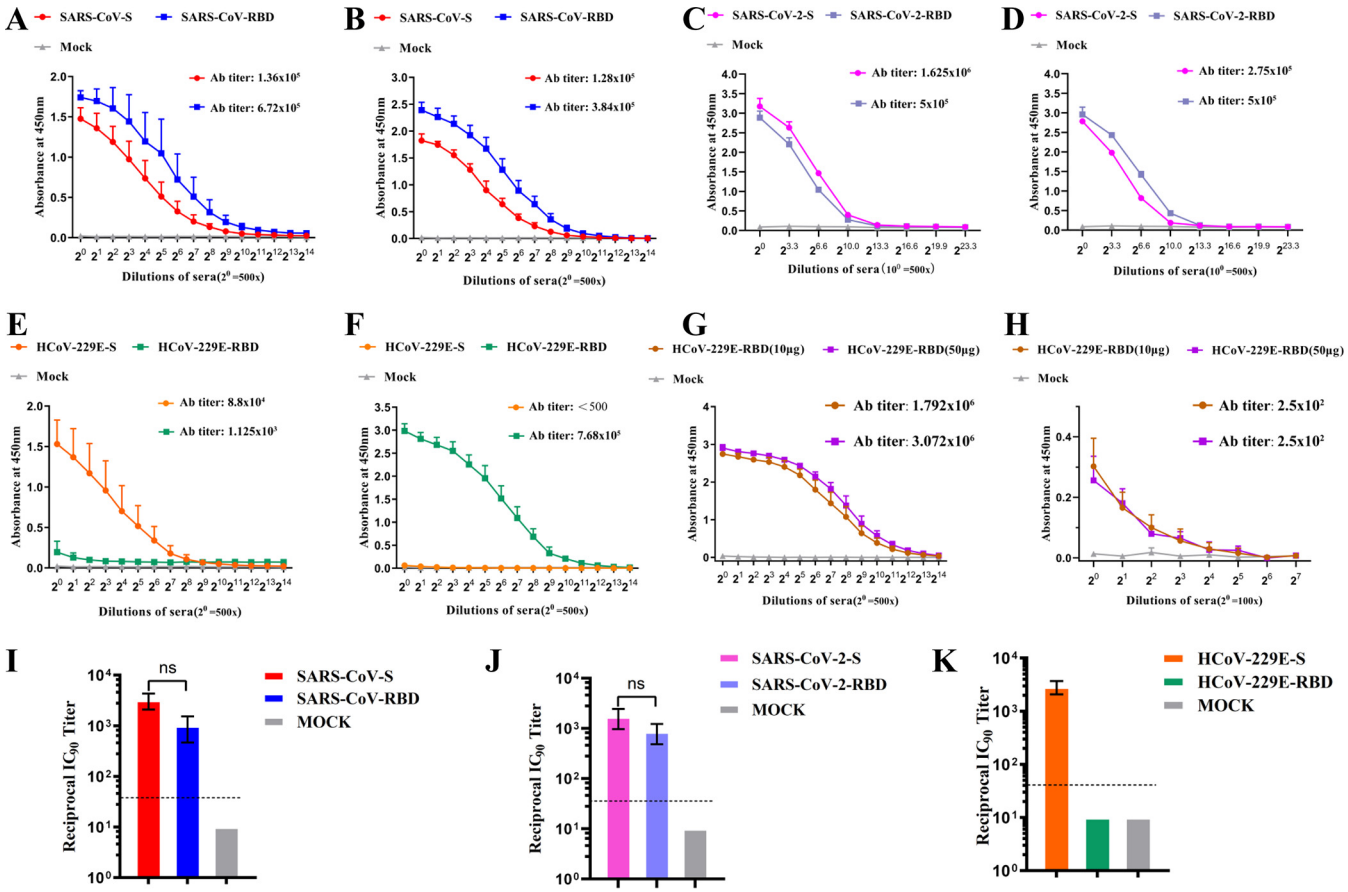

FIG 4 Immunological analysis of *Beta-CoV* (SARS-CoV and SARS-CoV-2) and *Alpha-CoV* (HCoV-229E) spike proteins. (A and B) Cross-reactivity of the SARS-CoV S-trimer and RBD-specific sera is measured using ELISA. Mouse sera for SARS-CoV S-trimer (red) and SARS-CoV RBD (blue) were 2-fold serially diluted and reacted with the S-trimer (A) or RBD (B), respectively. (C and D) Cross-reactivity of the SARS-CoV-2 S-trimer and RBD-specific sera is measured using ELISA. Mouse sera for SARS-CoV-2 S-trimer (magenta) and SARS-CoV-2 RBD (cyan) were 10-fold diluted and reacted with SARS-CoV-2 S-trimer (C) and RBD (D). (E and F) Cross-reactivity of the HCoV-229E S-trimer and RBD-specific sera is measured using ELISA. Mouse sera for HCoV-229E S-trimer (orange) and HCoV-229E RBD (green) were 2-fold diluted and reacted with HCoV-229E S-trimer (E) and RBD (F). (G and H) The antibody titers of sera from mice immunized with the HCoV-229E RBD (10 μg, brown; 50 μg, purple). Mouse sera were reacted with the HCoV-229E RBD (G) or S-trimer (H). Mouse sera were serially diluted from a 500-fold dilution. All the data are presented as the mean OD_{450} $\pm$ SD ($n = 3$), and the IgG antibody titers of each serum were calculated as the maximum endpoint dilution that remained positive. (I, J, and K) The neutralization assay of mouse sera from the S-trimer and RBD against SARS-CoV, SARS-CoV-2, and HCoV-229E pseudoviruses. The limit of detection for the assay depends on the initial dilution and is represented by dotted lines; a reciprocal IC_{90} titer of 40 was assigned. The data are presented as the mean reciprocal IC_{90} titer $\pm$ SD ($n = 3$). All differences between means with $P < 0.05$ are indicated. ns, not significant.

the S1 and NTD+RBD sera, while the NTD and RBD sera alone had no detectable neutralizing effects (Fig. 5B). Hence, our results indicate that the S1 region in the S-trimer should be the key region for NAb induction. To verify the importance of the complete S1 structure for NAb induction, we designed S-trimer mutants, namely, an NTD-deficient S-trimer (S-trimer/ΔNTD), the S1 subunit integrity of which was destroyed (Fig. 5C). Compared with HCoV-229E S-trimer (K_D value is 3.29 $\pm$ 0.0129 nM), *in vitro* binding measurements showed that S-trimer/ΔNTD has a similar binding affinity with hAPN (K_D value is 2.12 $\pm$ 0.15 nM) and functions well (Fig. 3B and Fig. 5D and E). However, the incomplete S1 conformation significantly reduces the level of NAbs induced by the S-trimer (Fig. 5F). Taken together, these results showed that the intact and stable S1 subunit in HCoV-229E S-trimer is a prerequisite for the production of effective NAbs.

Furthermore, our results showed that RBD functioned well *in vitro* (Fig. 3F), which indicates that the characteristics of RBD itself may lead to the generation of fewer neutralizing antibodies than S-trimer in HCoV-229E (Fig. 4K). Hence, we screened monoclonal antibodies using HCoV-229E S-trimer, and the results showed few antibodies targeting S1-RBD (Fig. 6A). To further determine the ability of RBD to induce antibodies itself, we screened monoclonal antibodies targeting the S1 region and found that the

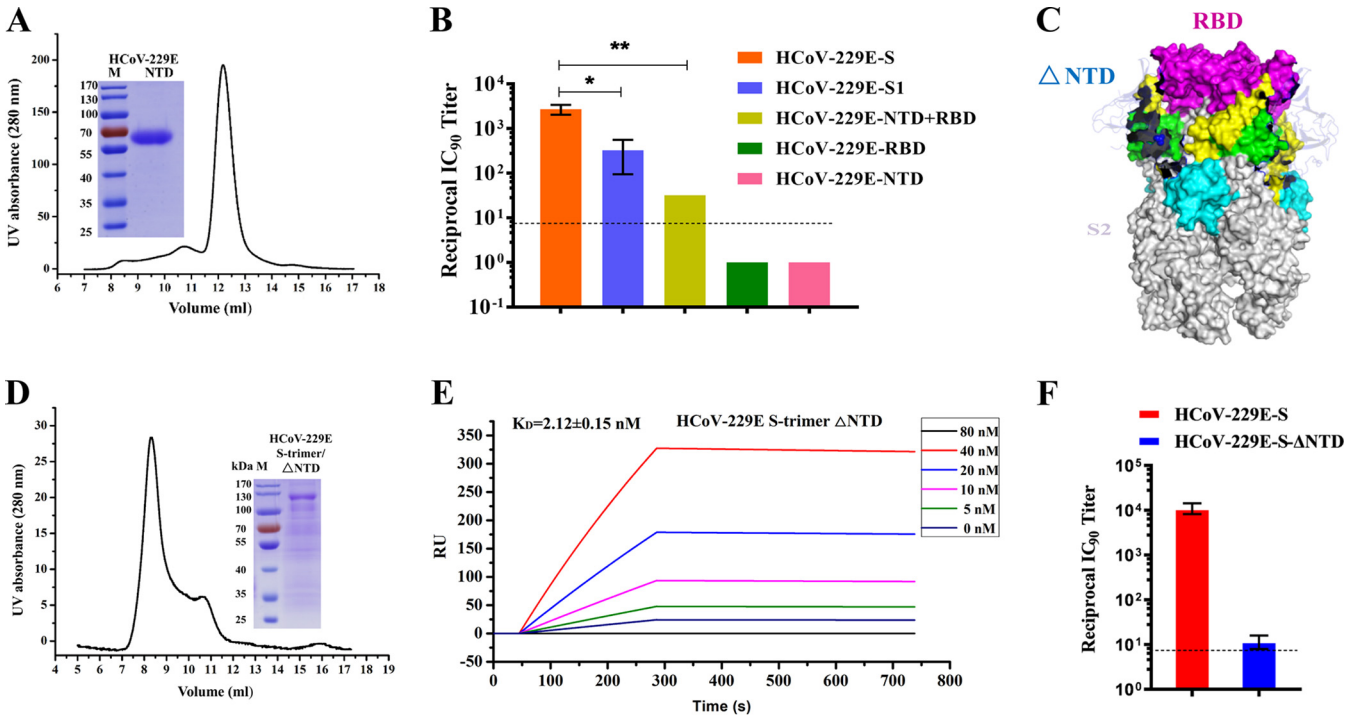

FIG 5 The intact and stable S1 subunit of HCoV-229E S-trimer is a prerequisite for the production of effective NAbs. (A and D) Oligomerization state analysis of spike proteins (HCoV-229E NTD and S-trimer/ΔNTD). Protein samples were eluted using a Superdex 200 10/300 GL column. The results of SDS-PAGE analysis are also shown. (B) The neutralization abilities of mouse sera from the HCoV-229E S-trimer, S1, NTD+RBD, NTD, and RBD against HCoV-229E strain VR740. (C) Structural model of HCoV-229E S-trimer/ΔNTD. The RBD, SD1, SD2, and S2 are colored in magenta, green, cyan, and gray, respectively. (E) Interactions of HCoV-229E S-trimer/ΔNTD and soluble hAPN. The detailed description is consistent with Fig. 3B. (F) The neutralization ability of mouse sera from HCoV-229E S-trimer/ΔNTD against HCoV-229E strain VR740. The data are presented as the mean reciprocal IC_{90} titer ± SD ($n = 3$). The limit of detection for the assay depends on the initial dilution and is represented by dotted lines; a reciprocal IC_{90} titer of 8 was assigned.

proportion of antibodies targeting RBD was approximately 20% (Fig. 6B). Since the S1 protein was expressed in a monomeric form, RBD is not restricted by the conformation of the surrounding domains and should be in a standing state. Therefore, our results indicate that HCoV-229E RBD may induce weaker levels of neutralizing antibodies,

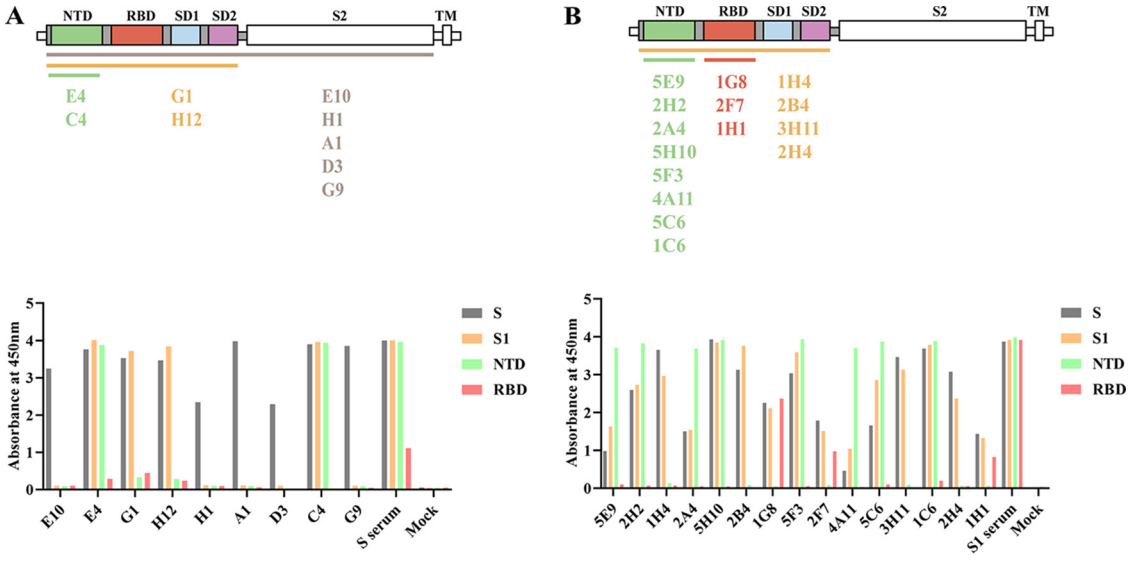

FIG 6 Monoclonal antibody epitope mapping of the HCoV-229E spike protein. Monoclonal antibody (MAb) epitope regions in the HCoV-229E spike protein (A) and S1 domain (B). Supernatants of positive hybridomas were reacted with the HCoV-229E spike protein, S1, NTD, and RBD. Data are presented as the OD_{450} (bottom). MAbs and their epitope regions are indicated below the schematic of the HCoV-229E spike protein.

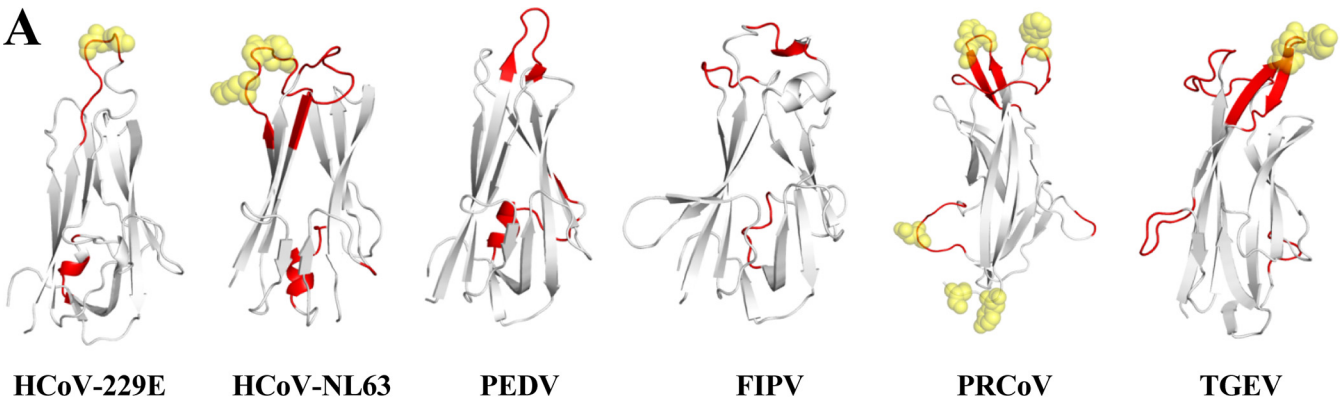

B

HCoV-229E *vs*	HCoV-NL63	PEDV	FIPV	PRCoV	TGEV
Dali Z-score	12.9	16.1	13.0	13.2	12.7
RMSD (Å)	1.7	1.8	2.4	3.2	3.3

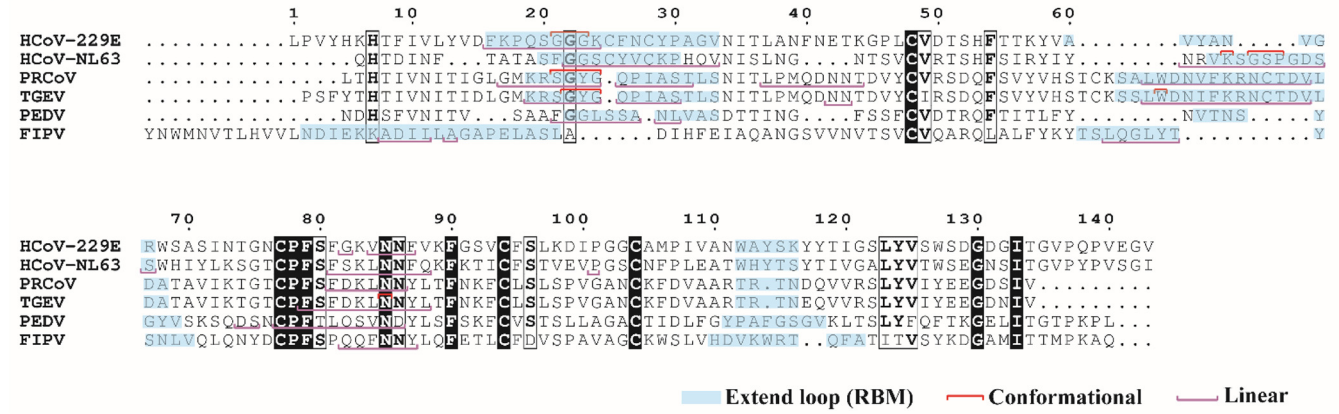

FIG 7 B-cell epitope analysis of alphacoronavirus S1-RBDs. (A) Structures of alphacoronavirus (HCoV-229E, HCoV-NL63, PEDV, FIPV, PRCoV, and TGEV) S1-RBDs. The linear (red cartoon) and conformational (yellow sphere) B-cell epitopes were predicted by Bepipred 2.0 or DiscoTope 2.0 and labeled into the corresponding structures by PyMOL. HCoV-229E (PDB ID: 6ATK), HCoV-NL63 (PDB ID: 3KBH), PEDV (PDB ID: 6U7K), FIPV (PDB ID: 6JX7), PRCoV (PDB ID: 4F5C), and TGEV (PDB ID: 4F2M). (B) Structural comparison of S1-RBDs between HCoV-229E and other alpha-CoVs (HCoV-NL63, PEDV, FIPV, PRCoV, and TGEV). (C) Sequence alignment of alphacoronavirus S1-RBDs. The RBM or putative RBM region is shown in cyan. The predicted amino acid residues for linear (purple) and conformational (red) B-cell epitopes are also shown.

which may be related to its own characteristics. Furthermore, the RBD in the HCoV-229E S-trimer is in the lying state. Its own characteristics and conformational states may prompt the HCoV-229E to escape the host's immune surveillance, thereby allowing itself to circulate in the population for a long time.

Potential vaccine strategies for *Alphacoronavirus* (HCoV-229E) and *Betacoronavirus* (SARS-CoV and SARS-CoV-2). We compared the structures of S-trimers and RBDs among alphacoronaviruses (Fig. 1B and Fig. 7A). We also predicted the potential B-cell epitopes for their RBDs (Fig. 7A; Table 1). In *Alpha-CoV*, the S-trimer had a closed S1 subunit with three lying RBDs (Fig. 1B). Moreover, the RBDs consist of a standard β-sandwich fold core and three short discontinuous loops in the same spatial region (12, 14, 16, 22, 26, 27, 38) (Fig. 7A). Meanwhile, we performed a structural conservative analysis and the results showed that the RBD structures of HCoV-NL63, PEDV, and FIPV were similar to HCoV-229E, with root mean square deviation (RMSD) values of 1.7, 1.8, and 2.4, respectively (Fig. 7B). Besides, the distribution of potential B-cell epitopes in the RBDs of alpha-CoVs was also similar to that of HCoV-229E (Fig. 7A and C; Table 1). Based on the above data, inherent differences exist in the RBDs between alpha- and

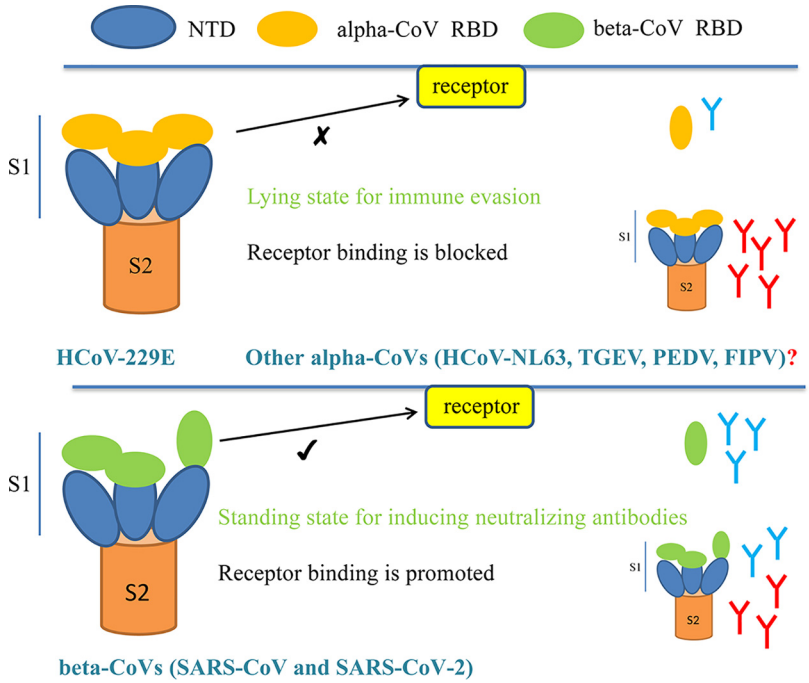

FIG 8 Potential vaccine strategies for alpha- and beta-CoVs. The model showed that the RBDs of the *alpha-CoV* S-trimers are in a lying state. In this state, the S protein cannot bind to the receptor, which is conducive to escaping the immune response targeting the RBD, and the HCoV-229E RBDs also induce fewer NAbs than beta-CoVs (SARS-CoV and SARS-CoV-2); thus, their S-trimers can be an effective potential subunit vaccine. In beta-CoVs (SARS-CoV and SARS-CoV-2), the RBDs of the S-trimer are in a standing state, which is conducive to binding receptors, and the RBD can induce more antibodies than HCoV-229E; thus, their S-trimers and RBDs can produce more NAbs. Hence, their S-trimers and RBDs can be an effective potential subunit vaccine.

beta-CoVs (Fig. 2 and Fig. 7A and B). However, the alpha- and beta-CoVs show high similarity in their RBDs and similar potential immune characteristics within their respective genera (Fig. 2, 4, and 7A and B). Accordingly, we speculate that in alpha-CoVs such as HCoV-229E, subunit vaccines should prioritize the S-trimer rather than the RBD; in beta-CoVs such as SARS-CoV and SARS-CoV-2, the S-trimer and RBD are both good candidates for subunit vaccines (Fig. 8).

In summary, we systematically analyzed the immunogenicity of the S-trimers and RBDs of *Alpha-CoV* (HCoV-229E) and *Beta-CoV* (SARS-CoV and SARS-CoV-2). Our results showed the inherent differences between the RBDs of alpha- and beta-CoVs and revealed potential identical immune characteristics in alpha- and beta-CoVs. Based on these findings, we provide potential vaccine strategies for alpha- and beta-CoVs. For alpha-CoVs, the S-trimer may be more suitable for subunit vaccines than the RBD. For beta-CoVs, SARS-CoV and SARS-CoV-2, the S-trimer and RBD are both candidates for subunit vaccines. Considering the potential influence of conformational states on immunogenicity, we will further evaluate the immunogenicity difference among the different aggregation states of S-trimer and RBD in the future. Although our inference requires more experimental data for further confirmation, our results will provide novel ideas for the development of coronavirus vaccines in the future.

MATERIALS AND METHODS

Plasmid construction. According to previous research, insect codon-optimized sequences encoding the HCoV-229E S glycoprotein ectodomain (GenBank accession number NP_073551.1, residues 1 to 1116; NTD-deficient S-trimer: S-trimer/ΔNTD) and SARS-CoV S glycoprotein ectodomain with an R667A mutation (GenBank accession number NP_828851.1, residues 1 to 1195) were cloned into the baculovirus transfer vector pFastbac1 (Invitrogen) with a gene fragment encoding the GCN4 trimerization motif (LIKRMKQIEDKIEEIESKQKKIENEIARIKKIK) and an eight-residue Strep tag (WSHPQFEK) (21, 23). The human aminopeptidase N (hAPN) (GenBank accession number JX869059, residues 66 to 967) (39) and human

ACE2 extracellular domain (residues 19 to 615) (40) were cloned into the pFastbac1 vector with an N-terminal honeybee melittin signal peptide and a C-terminal 6×His tag. Besides, HCoV-229E S1 (residues 1 to 536), S1-NTD (residues 1 to 258), S1-RBD (residues 295 to 428), and SARS-CoV S1-RBD (residues 306 to 527) containing an N-terminal honeybee melittin signal peptide and a C-terminal Fc tag were constructed using the same method (29). Besides, the S fragments of HCoV-229E, SARS-CoV, and SARS-CoV-2 were cloned into the pcDNA3.1 (+) vector with a C-terminal His tag using a previously described protocol (41). All constructs were validated using DNA sequencing. The sequences of S proteins (HCoV-229E, SARS-CoV, and SARS-CoV-2), hAPN, and hACE2 were synthesized by GenScript Corporation (GenScript, Nanjing, China).

Protein expression and purification. The spike protein ectodomain was expressed and purified using a previously described protocol (21, 29). Briefly, the construct was transformed into bacterial DH10Bac competent cells (Invitrogen); then, the extracted bacmid was transfected into Sf9 cells (American Type Culture Collection). The supernatant of the cell culture containing the secreted S glycoprotein was harvested at 60 h after infection and concentrated, and the buffer was changed to binding buffer (10 mM HEPES, pH 7.2, and 500 mM NaCl). The S-trimer (HCoV-229E and SARS-CoV) including Strep tag was captured using StrepTactin Sepharose high-performance resin (GE Healthcare) (21). HCoV-229E S1, S1-NTD, S1-RBD, and SARS-CoV S1-RBD including FC tag were harvested using a HiTrap Protein G HP column (GE Healthcare, Uppsala, Sweden). Besides, for SARS-CoV-2, the S-trimer (item no. 40589-V08B1) and S1-RBD (item no. 40592-V05H) were purchased from Sino Biological, Inc. In addition, the hAPN and hACE2 including His tag were harvested using HisTrap HP columns (GE Healthcare, Uppsala, Sweden). Finally, the harvested proteins were equilibrated with buffer (10 mM HEPES, pH 7.2, and 150 mM NaCl).

***In vitro* gel filtration analysis.** Oligomerization of the receptors (hAPN and hACE2), HCoV-229E S-trimer (wild type [WT], ΔNTD mutant), S1, S1-NTD, and S1-RBD, and SARS-CoV S-trimer and S1-RBD was analyzed using a Superdex 200 10/300 GL column (GE Healthcare) with a buffer containing 10 mM HEPES (pH 7.2) and 150 mM NaCl at a flow rate of 0.3 ml/min (4°C). Then, these proteins were analyzed by SDS-PAGE. The gel filtration results were analyzed using Origin 8.5 software.

Surface plasmon resonance. Binding kinetics of purified HCoV-229E S-trimer (WT, ΔNTD mutant), S1, and S1-RBD samples with the hAPN and purified SARS-CoV S-trimer and S1-RBD samples with the hACE2 were measured by surface plasmon resonance (OpenSPR; Nicoya Life), as described previously (42–44). Briefly, the hAPN or hACE2 (200 μl, 5 μg) was immobilized on the OpenSPR COOH sensor chip (Nicoya no. SEN-AU-100-12-COOH). Free activated carboxyl groups were deactivated with the addition of 100 μl blocking buffer (Nicoya). The immobilized protein was washed, the running buffer was injected for blank measurement followed by successive injections of buffer-matched HCoV-229E spike samples or SARS-CoV spike samples at 20 μl/min, the binding time was approximately 240 s, and the natural dissociation of approximately 400 s was carried out. Response unit (RU) values were measured at 298 K. Binding kinetic parameters were obtained by fitting the curve to a one-to-one binding model using the TraceDrawer software package (Ridgeview Instruments, Uppsala, Sweden). All injections were carried out in duplicate and gave essentially identical results. Only one of the duplicates is shown.

Animal immunization. Female BALB/c mice aged 6 weeks were immunized with different proteins at 0 and 3 weeks. Proteins (10 μg) diluted in HEPES-buffered saline (HBS; 10 mM HEPES and 150 mM NaCl) were mixed 1:1 with the 2×Sigma adjuvant system. The mice were intramuscularly inoculated with 50 μl of this solution (25 μl into each hind leg). Two weeks after the final immunization, sera were collected for subsequent assays. For SARS-CoV-2, the corresponding rabbit polyclonal antibodies (PAbs) were purchased from Sino Biological, Inc.

Enzyme-linked immunosorbent assay (ELISA). To measure the immune responses of different sera, ELISA plates were coated with purified protein at 0.1 μM/well in citrate-buffered saline (CBS, pH 9.6) overnight at 4°C and subsequently blocked with phosphate-buffered saline (PBS) with 0.05% Tween 20 (PBST) containing 1% (wt/vol) bovine serum albumin (BSA) at 37°C. After standard washes, the plates were incubated with 2- or 10-fold serially diluted sera for 1 h at 37°C. Then, horseradish peroxidase (HRP)-conjugated goat anti-mouse/rabbit IgG (1:10,000 diluted in PBST with 1% [wt/vol] BSA; Boster) was used as the secondary antibody, and 3,3′,5,5′-tetramethylbenzidine (TMB) (Beyotime) was used as the substrate for detection. Optical density (OD) was determined at 450 nm and 630 nm using a Spark 10M microplate reader (Tecan) after stopping the reaction with 2 M H_2SO_4. Serum from mice immunized with HBS was used as a control.

Generation of HCoV-229E S protein MAbs and epitope mapping. Six-week-old female BALB/c mice were immunized with 100 μg of purified HCoV-229E S-trimer or S1 protein. Antigens were emulsified in Freund's complete adjuvant (Sigma-Aldrich; F5881) for the first immunization or Freund's incomplete adjuvant (Sigma-Aldrich; F5506) for the subsequent boost. Each mouse received three subcutaneous injections at 2-week intervals. Mice with the highest titers of antibodies against the HCoV-229E S-trimer or S1 protein were further boosted by intraperitoneal injection of 200 μg of purified HCoV-229E S-trimer or S1 protein diluted in PBS buffer. Three days after the last injection, spleen cells were collected and fused with SP2/0 cells with PEG1450 (Sigma-Aldrich; P7181) to generate hybridoma cells. Antigen-specific ELISA was used for the hybridoma screening. Positive hybridomas were further subcloned and used for epitope mapping. Finally, ELISA plates were coated with different proteins (the HCoV-229E S-trimer, S1, S1-NTD, and S1-RBD) at 1 μg/ml in CBS (pH 9.6) overnight at 4°C and subsequently blocked and washed. Then, the plates were reacted with the hybridoma culture supernatants at 37°C for 1 h. HRP-conjugated goat anti-mouse IgG (1:5,000 diluted in PBST with 1% [wt/vol] BSA; Boster) was used for detection. Signal reading was carried out in the manner described above. Hybridoma culturing medium was used as a control.

Pseudotyped-virus neutralization assay. In this study, HCoV-229E (ATCC, VR-740) was amplified using Huh7 cells, and pseudotyped viruses were produced as previously described (41). The HEK-293T cells were transfected with 1 μg of HCoV-229E-S-Δ19-pcDNA3.1 (C-terminal deletion 19 amino acids [aa]), SARS-CoV-S-Δ22-pcDNA3.1 (C-terminal deletion 22 aa), and SARS-CoV-2-S-Δ18-pcDNA3.1 (C-terminal deletion 18 aa) plasmids using Exfect2000 transfection reagent (Vazyme). Besides, VSV-G-pcDNA3.1 and pcDNA3.1 were transfected as positive and negative controls, respectively. Then, the transfected cells were infected with VSV-ΔG-G at a multiplicity of infection (MOI) of 1. After 24 h, VSV-ΔG-HCoV-229E-S, VSV-ΔG-SARS-CoV-S, and VSV-ΔG-SARS-CoV-2-S (culture supernatants) were harvested and stored at −80°C until use.

For titration of these three pseudoviruses, 10-fold dilution was performed in 96-well culture plates. The cell with added pcDNA3.1-transfected supernatant was used as a control. After 48 h, the culture supernatant was removed and washed using PBS, and 20 μl of reporter lysis 5×Buffer (Promega; catalog no. E4030) was added to each well. Then, the luciferase substrate (Promega; catalog no. E1500) was added, and the luminescence activity was measured using a multimode microplate reader (Tecan Spark 10M). The viral titers were calculated using the Reed-Muench method.

For pseudovirus neutralization assay, 2-fold serial dilutions of mouse sera (initially 1:40) were mixed with the pseudovirus strains (HCoV-229E, SARS-CoV, and SARS-CoV-2; 100 $TCID_{50}$/well). After 48 h, the luminescence activity was measured. According to the formula $(V - X)/(V - C) \times 100\%$ (where X is sample reading, C is cell control reading, and V is virus control reading; $n = 3$), the neutralization protection rate (90% inhibitory concentration [IC_{90}]) was calculated. Besides, for virus neutralization assay, 2-fold serial dilutions of mouse sera (initially 1:8) were mixed with an equal volume of HCoV-229E (ATCC, VR-740, 100 $TCID_{50}$/well) at 37°C. After 5 days of incubation, the cytopathic effect (CPE) was observed by an inverted optical microscope. The highest serum dilution that protected more than 90% of cells from CPE was taken as the neutralization titer (IC_{90}). Serum from mice immunized with HBS was used as a control.

B-cell epitope prediction analysis. According to previous research, B-cell epitopes were predicted and analyzed (IEDB, https://www.iedb.org/) (45). Briefly, structure-based B-cell epitope prediction was performed by DiscoTope 2.0 with a positive cutoff greater than −3.7 (corresponding to a specificity greater than or equal to 0.75 and a sensitivity less than 0.47) using the following protein structures: the HCoV-229E S-trimer and RBD (PDB IDs: 6U7H and 6ATK, respectively), the SARS-CoV S-trimer and RBD (PDB IDs: 5X5B and 2AJF, respectively), the SARS-CoV-2 S-trimer and RBD (PDB IDs: 6VYB and 6M0J, respectively), the HCoV-NL63 (PDB ID: 3KBH), the PEDV RBD (PDB ID: 6U7K), the FIPV RBD (PDB ID: 6JX7), the porcine respiratory coronavirus (PRCoV) RBD (PDB ID: 4F5C), and the transmissible gastroenteritis virus (TGEV) RBD (PDB ID: 4F2M). For linear B-cell epitope prediction, the corresponding amino acid sequences from the above structures were used. The BepiPred 2.0 algorithm was applied with a cutoff of 0.55 (corresponding to a specificity greater than 0.81 and a sensitivity less than 0.3). All the predicted residues were labeled in corresponding structures using PyMOL (Schrödinger). Besides, the interaction area and surface area were analyzed via PDBePISA (https://www.ebi.ac.uk/msd-srv/prot_int/pistart.html). Additionally, the amino acid sequences of alpha-CoV RBDs were aligned using ClustalW2 (46). The NCBI accession numbers of the sequences used were as follows: HCoV-229E (AAQ90002.1), HCoV-NL63 (AVL25587.1), PRCoV (AAA46905.1), TGEV (CAB91145.1), PEDV (AIU98611.1), and FIPV (ACT10887.1).

Statistical analysis. Statistical analysis was carried out using GraphPad Prism 7.0. Statistical analysis was conducted on data from three independent experimental replicates. Statistical significance was determined using an unpaired two-tailed Student t test. Data are presented as mean values ± SD (95% confidence interval). All differences between means with $P < 0.05$ are indicated. * indicates $P < 0.05$, which was considered significant, and ** indicates $P < 0.01$, which was considered highly significant.

Ethics statement. All the mice used in this study were maintained in compliance with the recommendations in the Regulations for the Administration of Affairs Concerning Experimental Animals established by the Ministry of Science and Technology of China. The experiments were carried out using the protocols approved by the Scientific Ethics Committee of Huazhong Agricultural University (permit number: HZAUSW-2018-009).

ACKNOWLEDGMENTS

This work was supported by National Key R&D Plan of China grant 2018YFD0500100, National Natural Science Foundation of China grants 31722056 and 31702249, China Postdoctoral Science Foundation grant 2019M662674, and the Huazhong Agricultural University Scientific and Technological Self-innovation Foundation (program no. 2662017PY028).

We declare no competing interests.

REFERENCES

1. Adams MJ, Lefkowitz EJ, King AM, Bamford DH, Breitbart M, Davison AJ, Ghabrial SA, Gorbalenya AE, Knowles NJ, Krell P, Lavigne R, Prangishvili D, Sanfaçon H, Siddell SG, Simmonds P, Carstens EB. 2015. Ratification vote on taxonomic proposals to the International Committee on Taxonomy of Viruses (2015). Arch Virol 160:1837–1850. https://doi.org/10.1007/s00705-015-2425-z.
2. Cui J, Li F, Shi ZL. 2019. Origin and evolution of pathogenic coronaviruses. Nat Rev Microbiol 17:181–192. https://doi.org/10.1038/s41579-018-0118-9.
3. Su S, Wong G, Shi W, Liu J, Lai ACK, Zhou J, Liu W, Bi Y, Gao GF. 2016. Epidemiology, genetic recombination, and pathogenesis of coronaviruses. Trends Microbiol 24:490–502. https://doi.org/10.1016/j.tim.2016.03.003.
4. Huang C, Wang Y, Li X, Ren L, Zhao J, Hu Y, Zhang L, Fan G, Xu J, Gu X,

Cheng Z, Yu T, Xia J, Wei Y, Wu W, Xie X, Yin W, Li H, Liu M, Xiao Y, Gao H, Guo L, Xie J, Wang G, Jiang R, Gao Z, Jin Q, Wang J, Cao B. 2020. Clinical features of patients infected with 2019 novel coronavirus in Wuhan, China. Lancet 395:497–506. https://doi.org/10.1016/S0140-6736(20)30183-5.
5. Kin N, Miszczak F, Lin W, Gouilh MA, Vabret A, EPICOREM Consortium. 2015. Genomic analysis of 15 human coronaviruses OC43 (HCoV-OC43s) circulating in France from 2001 to 2013 reveals a high intra-specific diversity with new recombinant genotypes. Viruses 7:2358–2377. https://doi.org/10.3390/v7052358.
6. Monto AS. 1974. Medical reviews. Coronaviruses. Yale J Biol Med 47:234–251.
7. Coronaviridae Study Group of the International Committee on Taxonomy of Viruses. 2020. The species Severe acute respiratory syndrome-related coronavirus: classifying 2019-nCoV and naming it SARS-CoV-2. Nat Microbiol 5:536–544. https://doi.org/10.1038/s41564-020-0695-z.
8. Raj VS, Osterhaus AD, Fouchier RA, Haagmans BL. 2014. MERS: emergence of a novel human coronavirus. Curr Opin Virol 5:58–62. https://doi.org/10.1016/j.coviro.2014.01.010.
9. Peiris JS, Lai ST, Poon LL, Guan Y, Yam LY, Lim W, Nicholls J, Yee WK, Yan WW, Cheung MT, Cheng VC, Chan KH, Tsang DN, Yung RW, Ng TK, Yuen KY. 2003. Coronavirus as a possible cause of severe acute respiratory syndrome. Lancet 361:1319–1325. https://doi.org/10.1016/S0140-6736(03)13077-2.
10. Zaki AM, van Boheemen S, Bestebroer TM, Osterhaus AD, Fouchier RA. 2012. Isolation of a novel coronavirus from a man with pneumonia in Saudi Arabia. N Engl J Med 367:1814–1820. https://doi.org/10.1056/NEJMoa1211721.
11. Li F. 2016. Structure, function, and evolution of coronavirus spike proteins. Annu Rev Virol 3:237–261. https://doi.org/10.1146/annurev-virology-110615-042301.
12. Yang TJ, Chang YC, Ko TP, Draczkowski P, Chien YC, Chang YC, Wu KP, Khoo KH, Chang HW, Hsu SD. 2020. Cryo-EM analysis of a feline coronavirus spike protein reveals a unique structure and camouflaging glycans. Proc Natl Acad Sci U S A 117:1438–1446. https://doi.org/10.1073/pnas.1908898117.
13. Wrapp D, Wang N, Corbett KS, Goldsmith JA, Hsieh CL, Abiona O, Graham BS, McLellan JS. 2020. Cryo-EM structure of the 2019-nCoV spike in the prefusion conformation. Science 367:1260–1263. https://doi.org/10.1126/science.abb2507.
14. Wrapp D, McLellan JS. 2019. The 3.1-angstrom cryo-electron microscopy structure of the porcine epidemic diarrhea virus spike protein in the prefusion conformation. J Virol 93:e00923-19. https://doi.org/10.1128/JVI.00923-19.
15. Tortorici MA, Walls AC, Lang Y, Wang C, Li Z, Koerhuis D, Boons GJ, Bosch BJ, Rey FA, de Groot RJ, Veesler D. 2019. Structural basis for human coronavirus attachment to sialic acid receptors. Nat Struct Mol Biol 26:481–489. https://doi.org/10.1038/s41594-019-0233-y.
16. Li Z, Tomlinson AC, Wong AH, Zhou D, Desforges M, Talbot PJ, Benlekbir S, Rubinstein JL, Rini JM. 2019. The human coronavirus HCoV-229E S-protein structure and receptor binding. Elife 8:e51230. https://doi.org/10.7554/eLife.51230.
17. Xiong X, Tortorici MA, Snijder J, Yoshioka C, Walls AC, Li W, McGuire AT, Rey FA, Bosch BJ, Veesler D. 2018. Glycan shield and fusion activation of a deltacoronavirus spike glycoprotein fine-tuned for enteric infections. J Virol 92:e01628-17. https://doi.org/10.1128/JVI.01628-17.
18. Shang J, Zheng Y, Yang Y, Liu C, Geng Q, Tai W, Du L, Zhou Y, Zhang W, Li F. 2018. Cryo-electron microscopy structure of porcine deltacoronavirus spike protein in the prefusion state. J Virol 92:e01556-17. https://doi.org/10.1128/JVI.01556-17.
19. Shang J, Zheng Y, Yang Y, Liu C, Geng Q, Luo C, Zhang W, Li F. 2018. Cryo-EM structure of infectious bronchitis coronavirus spike protein reveals structural and functional evolution of coronavirus spike proteins. PLoS Pathog 14:e1007009. https://doi.org/10.1371/journal.ppat.1007009.
20. Yuan Y, Cao D, Zhang Y, Ma J, Qi J, Wang Q, Lu G, Wu Y, Yan J, Shi Y, Zhang X, Gao GF. 2017. Cryo-EM structures of MERS-CoV and SARS-CoV spike glycoproteins reveal the dynamic receptor binding domains. Nat Commun 8:15092. https://doi.org/10.1038/ncomms15092.
21. Gui M, Song W, Zhou H, Xu J, Chen S, Xiang Y, Wang X. 2017. Cryo-electron microscopy structures of the SARS-CoV spike glycoprotein reveal a prerequisite conformational state for receptor binding. Cell Res 27:119–129. https://doi.org/10.1038/cr.2016.152.
22. Walls AC, Tortorici MA, Frenz B, Snijder J, Li W, Rey FA, DiMaio F, Bosch BJ, Veesler D. 2016. Glycan shield and epitope masking of a coronavirus spike protein observed by cryo-electron microscopy. Nat Struct Mol Biol 23:899–905. https://doi.org/10.1038/nsmb.3293.
23. Walls AC, Tortorici MA, Bosch BJ, Frenz B, Rottier PJM, DiMaio F, Rey FA, Veesler D. 2016. Cryo-electron microscopy structure of a coronavirus spike glycoprotein trimer. Nature 531:114–117. https://doi.org/10.1038/nature16988.
24. Kirchdoerfer RN, Cottrell CA, Wang N, Pallesen J, Yassine HM, Turner HL, Corbett KS, Graham BS, McLellan JS, Ward AB. 2016. Pre-fusion structure of a human coronavirus spike protein. Nature 531:118–121. https://doi.org/10.1038/nature17200.
25. Du L, He Y, Zhou Y, Liu S, Zheng BJ, Jiang S. 2009. The spike protein of SARS-CoV–a target for vaccine and therapeutic development. Nat Rev Microbiol 7:226–236. https://doi.org/10.1038/nrmicro2090.
26. Wong AHM, Tomlinson ACA, Zhou D, Satkunarajah M, Chen K, Sharon C, Desforges M, Talbot PJ, Rini JM. 2017. Receptor-binding loops in alphacoronavirus adaptation and evolution. Nat Commun 8:1735. https://doi.org/10.1038/s41467-017-01706-x.
27. Wu K, Li W, Peng G, Li F. 2009. Crystal structure of NL63 respiratory coronavirus receptor-binding domain complexed with its human receptor. Proc Natl Acad Sci U S A 106:19970–19974. https://doi.org/10.1073/pnas.0908837106.
28. Lan J, Ge J, Yu J, Shan S, Zhou H, Fan S, Zhang Q, Shi X, Wang Q, Zhang L, Wang X. 2020. Structure of the SARS-CoV-2 spike receptor-binding domain bound to the ACE2 receptor. Nature 581:215–220. https://doi.org/10.1038/s41586-020-2180-5.
29. Li F, Li W, Farzan M, Harrison SC. 2005. Structure of SARS coronavirus spike receptor-binding domain complexed with receptor. Science 309:1864–1868. https://doi.org/10.1126/science.1116480.
30. Wang N, Shi X, Jiang L, Zhang S, Wang D, Tong P, Guo D, Fu L, Cui Y, Liu X, Arledge KC, Chen YH, Zhang L, Wang X. 2013. Structure of MERS-CoV spike receptor-binding domain complexed with human receptor DPP4. Cell Res 23:986–993. https://doi.org/10.1038/cr.2013.92.
31. Pallesen J, Wang N, Corbett KS, Wrapp D, Kirchdoerfer RN, Turner HL, Cottrell CA, Becker MM, Wang L, Shi W, Kong WP, Andres EL, Kettenbach AN, Denison MR, Chappell JD, Graham BS, Ward AB, McLellan JS. 2017. Immunogenicity and structures of a rationally designed prefusion MERS-CoV spike antigen. Proc Natl Acad Sci U S A 114:E7348–E7357. https://doi.org/10.1073/pnas.1707304114.
32. Lan J, Yao Y, Deng Y, Chen H, Lu G, Wang W, Bao L, Deng W, Wei Q, Gao GF, Qin C, Tan W. 2015. Recombinant receptor binding domain protein induces partial protective immunity in rhesus macaques against Middle East respiratory syndrome coronavirus challenge. EBioMedicine 2:1438–1446. https://doi.org/10.1016/j.ebiom.2015.08.031.
33. He Y, Li J, Heck S, Lustigman S, Jiang S. 2006. Antigenic and immunogenic characterization of recombinant baculovirus-expressed severe acute respiratory syndrome coronavirus spike protein: implication for vaccine design. J Virol 80:5757–5767. https://doi.org/10.1128/JVI.00083-06.
34. Yang J, Wang W, Chen Z, Lu S, Yang F, Bi Z, Bao L, Mo F, Li X, Huang Y, Hong W, Yang Y, Zhao Y, Ye F, Lin S, Deng W, Chen H, Lei H, Zhang Z, Luo M, Gao H, Zheng Y, Gong Y, Jiang X, Xu Y, Lv Q, Li D, Wang M, Li F, Wang S, Wang G, Yu P, Qu Y, Yang L, Deng H, Tong A, Li J, Wang Z, Yang J, Shen G, Zhao Z, Li Y, Luo J, Liu H, Yu W, Yang M, Xu J, Wang J, Li H, Wang H, et al. 2020. A vaccine targeting the RBD of the S protein of SARS-CoV-2 induces protective immunity. Nature 586:572–577. https://doi.org/10.1038/s41586-020-2599-8.
35. Liu X, Drelich A, Li W, Chen C, Sun Z, Shi M, Adams C, Mellors JW, Tseng CT, Dimitrov DS. 2020. Enhanced elicitation of potent neutralizing antibodies by the SARS-CoV-2 spike receptor binding domain Fc fusion protein in mice. Vaccine 38:7205–7212. https://doi.org/10.1016/j.vaccine.2020.09.058.
36. Chen WH, Tao X, Agrawal AS, Algaissi A, Peng BH, Pollet J, Strych U, Bottazzi ME, Hotez PJ, Lustigman S, Du L, Jiang S, Tseng CK. 2020. Yeast-expressed SARS-CoV recombinant receptor-binding domain (RBD219-N1) formulated with aluminum hydroxide induces protective immunity and reduces immune enhancement. Vaccine 38:7533–7541. https://doi.org/10.1016/j.vaccine.2020.09.061.
37. Kirchdoerfer RN, Wang N, Pallesen J, Wrapp D, Turner HL, Cottrell CA, Corbett KS, Graham BS, McLellan JS, Ward AB. 2018. Stabilized coronavirus spikes are resistant to conformational changes induced by receptor recognition or proteolysis. Sci Rep 8:15701. https://doi.org/10.1038/s41598-018-34171-7.
38. Reguera J, Santiago C, Mudgal G, Ordoño D, Enjuanes L, Casasnovas JM. 2012. Structural bases of coronavirus attachment to host aminopeptidase N and its inhibition by neutralizing antibodies. PLoS Pathog 8:e1002859. https://doi.org/10.1371/journal.ppat.1002859.
39. Wong AH, Zhou D, Rini JM. 2012. The X-ray crystal structure of human aminopeptidase N reveals a novel dimer and the basis for peptide

processing. J Biol Chem 287:36804–36813. https://doi.org/10.1074/jbc.M112.398842.
40. Song W, Gui M, Wang X, Xiang Y. 2018. Cryo-EM structure of the SARS coronavirus spike glycoprotein in complex with its host cell receptor ACE2. PLoS Pathog 14:e1007236. https://doi.org/10.1371/journal.ppat.1007236.
41. Wang J, Deng F, Ye G, Dong W, Zheng A, He Q, Peng G. 2016. Comparison of lentiviruses pseudotyped with S proteins from coronaviruses and cell tropisms of porcine coronaviruses. Virol Sin 31:49–56. https://doi.org/10.1007/s12250-015-3690-4.
42. Zhao N, Kamijo K, Fox PD, Oda H, Morisaki T, Sato Y, Kimura H, Stasevich TJ. 2019. A genetically encoded probe for imaging nascent and mature HA-tagged proteins in vivo. Nat Commun 10:2947. https://doi.org/10.1038/s41467-019-10846-1.
43. Song T, Yang Y, Wei H, Xie X, Lu J, Zeng Q, Peng J, Zhou Y, Jiang S, Peng J. 2019. Zfp217 mediates m6A mRNA methylation to orchestrate transcriptional and post-transcriptional regulation to promote adipogenic differentiation. Nucleic Acids Res 47:6130–6144. https://doi.org/10.1093/nar/gkz312.
44. Fang Q, Andrews J, Sharma N, Wilk A, Clark J, Slyskova J, Koczor CA, Lans H, Prakash A, Sobol RW. 2019. Stability and sub-cellular localization of DNA polymerase β is regulated by interactions with NQO1 and XRCC1 in response to oxidative stress. Nucleic Acids Res 47:6269–6286. https://doi.org/10.1093/nar/gkz293.
45. Grifoni A, Sidney J, Zhang Y, Scheuermann RH, Peters B, Sette A. 2020. A sequence homology and bioinformatic approach can predict candidate targets for immune responses to SARS-CoV-2. Cell Host Microbe 27:671–680.e2. https://doi.org/10.1016/j.chom.2020.03.002.
46. Larkin MA, Blackshields G, Brown NP, Chenna R, McGettigan PA, McWilliam H, Valentin F, Wallace IM, Wilm A, Lopez R, Thompson JD, Gibson TJ, Higgins DG. 2007. Clustal W and Clustal X version 2.0. Bioinformatics 23:2947–2948. https://doi.org/10.1093/bioinformatics/btm404.